Turbulent Heat Transfer From a Slot Jet Impinging on a Flat Plate

Dahbia Benmouhoub
e-mail: benmouhoub_d@yahoo.com

Amina Mataoui
e-mail: amataoui@gmail.com

Laboratoire de Mécanique des Fluides
Théorique et Appliquée,
Faculté de Physique,
Université des sciences et de la
technologie Houari Boumediene,
B.P. 32, Bab Ezzouar,
16111 Al Alia, Alger, Algérie

The flow field and heat transfer of a plane impinging jet on a hot moving wall were investigated using one point closure turbulence model. Computations were carried out by means of a finite volume method. The evolutions of mean velocity components, vorticity, skin friction coefficient, Nusselt number and pressure coefficient are examined in this paper. Two parameters of this type of interaction are considered for a given impinging distance of 8 times the nozzle thickness ($H/e = 8$): the jet-surface velocity ratio and the jet exit Reynolds number. The flow field structure at a given surface-to-jet velocity ratio is practically independent to the jet exit Reynolds number. A slight modification of the flow field is observed for weak surface-to-jet velocity ratios while the jet is strongly driven for higher velocity ratio. The present results satisfactorily compare to the experimental data available in the literature for $R_{sj} \leq 1$.The purpose of this paper is to investigate this phenomenon for higher R_{sj} values ($0 \leq R_{sj} \leq 4$). It follows that the variation of the mean skin friction and the Nusselt number can be correlated according to the surface-to-jet velocity ratios and the Reynolds numbers. [DOI: 10.1115/1.4024554]

Keywords: slot jet, impinging, moving wall, turbulent flow, heat transfer

1 Introduction

Impinging jets are extensively investigated in numerous benchmarks. Such configurations are common in many industrial and engineering applications (e.g., manufacturing, material processing, electronic cooling, paper drying, textiles and tempering of glass). Various comprehensive reviews of jets impingement onto a motionless wall are available in the literature [1–9]. However, a small number of studies were devoted to the effects of the wall motion of impinging jets, on the flow structure and the heat transfer.

The first study of a jet impingement on a moving wall was carried out experimentally by Subba Raju and Schlünder [10]. They investigated the heat transfer of a single jet impinging a moving belt. Huang et al. [11] performed numerically the case of a turbulent jet on a rectangular duct with surface motion effects. They have found that, when the plate velocity is great, Nusselt numbers becomes smaller around the area where the surface motion is opposed to that of the flow and augments when the moving wall and the flow evolve in the same direction. Zumbrunnen [12] have developed an analytical study for a single planar laminar impinging slot jet onto a moving plate subjected to a constant heat flux.-They show that the heat transfer is more effective when the boundary layer development is slowed down by the plate motion. Chattopadhyay et al. [13] have numerically investigated the turbulent heat transfer of an array of slot jets impinging a moving plate using large Eddy simulation (LES), for jet exit Reynolds numbers ranging between 500 and 3000 and for several surface-jet velocities ratios R_{sj} such as: $0 \leq R_{sj} \leq 2$. They found that the Nusselt number distribution over the plate becomes more uniform when the total heat transfer and the plate velocity decreases. Later, Chattopadhyay and Saha [14] used large Eddy simulation to investigate both the turbulent flow and the heat transfer resulting from a single slot jet impingement onto a moving hot isothermal plate. They have provided some results for a given jet exit Reynolds number of 5800 on a moving plate corresponding to a velocity ratio between 0 and 2. They were focused on the details of the flow structure, the velocity profiles and the turbulent shear stresses distribution. Similarly, the flow field of a confined turbulent slot air jet impinging perpendicularly a flat surface, was experimentally studied by Senter [15]. The experiments were carried out for a nozzle-to-plate spacing of eight slot nozzle thickness, at three Reynolds number (5300, 8000, and 10,600) and four surface-to-jet velocity ratios (0, 0.25, 0.5 and 1.0). Measurements are performed within the main regions of the jet. It appears that the flow structure patterns corresponding to a given surface-to-jet velocity ratio are independent with the jet exit Reynolds number between 5300 and 10,600. Also, a slight modification of the flow field is observed for a surface-to-jet velocity ratio of 0.25, whereas this effect is more significant for higher ratios of 0.5 and 1. On the other hand, Senter [15], determined the local Nusselt number by means the computation fluid dynamics (CFD) software Fluent using k–ε WCP model for jet exit Reynolds number of $\mathrm{Re} = 10{,}600$ and normalized plate velocities of 0, 0.25, 0.5, and 1.0. This study proves that the local Nusselt number tends to significantly decrease followed by an increasing around the stagnation zone. Sharif and Banerjee [16] have achieved a numerical study by the CFD code Fluent, using the standard k–ε turbulence model coupled to the enhanced wall treatment. They showed that the local Nusselt numbers along the moving plate exceed the values in the vicinity of the impinging region for the cases corresponding to lower plate velocities ratios, which can be explained by the thinning of dynamical and thermal boundary layers. These values decrease for greatest plate velocities induced by the parallel dominating shear driven flow. For a given plate velocity, the average Nusselt number close to the plate augments whilst the average skin friction coefficient decreases when jet exit Reynolds number increases. On the other hand, for a given jet exit Reynolds number, these two parameters slightly decrease for small velocity ratio, followed by an increase for greater values In the present paper, the case of a confined slot jet impinging perpendicularly a moving heated wall is numerically investigated (Fig. 1). This study complements both the previous work of Senter [15] and Sharif and Banerjee [16] by considering values of jet-plate velocity ratios greater than 1 ($0 \leq R_{sj} \leq 4$). We extend the velocity ratio surface-jet because Zumbrunnen et al. [17] reported that the impingement surface

Contributed by the Heat Transfer Division of ASME for publication in the Journal of Heat Transfer. Manuscript received July 3, 2012; final manuscript received May 3, 2013; published online August 19, 2013. Assoc. Editor: Wilson K. S. Chiu.

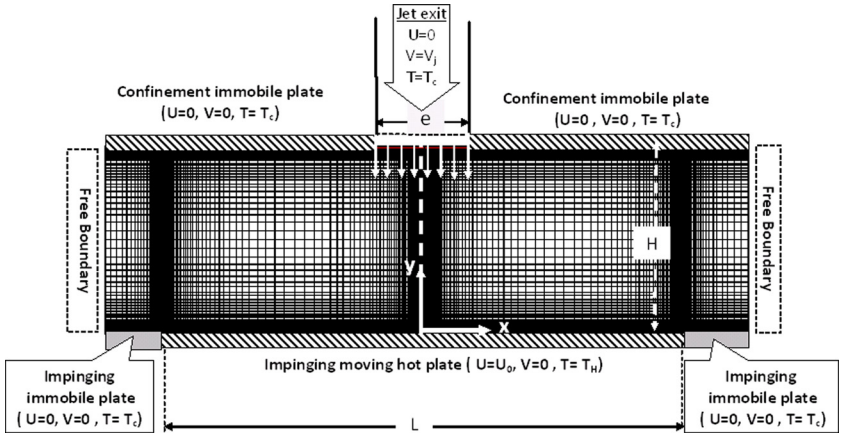

Fig. 1 Configuration and parameters

velocity can exceed as much as ten (10) times the jet velocity in some industrial application such as hot rolling process.

2 Methodology

Reynolds averaged equations can be written using transport conservative equations (mass Eq. (1), momentum Eq. (2) and energy Eq. (3)) form required by finite volume method

$$\frac{\partial U_i}{\partial x_i} = 0 \tag{1}$$

$$U_j \frac{\partial U_i}{\partial x_j} = -\frac{\partial}{\partial x_i}\left(\frac{\overline{P}}{\rho}\right) + \frac{\partial}{\partial x_j}\left(\nu \frac{\partial U_i}{\partial x_j} - \overline{u_i u_j}\right) \tag{2}$$

$$\rho U_i \frac{\partial T}{\partial x_i} = \frac{\partial}{\partial x_i}\left(\frac{\mu}{p_r}\frac{\partial T}{\partial x_i} - \rho \overline{u_i \theta}\right) \tag{3}$$

The closure of Reynolds Average Navier Stokes (RANS) equations is achieved through the standard k–ω model which takes into account some modifications due to low-Reynolds numbers effects and shear flow spreading [18]. The transport equations of the turbulent kinetic energy (k) and the specific dissipation rate (ω) are, respectively, written as

$$\rho U_j \frac{\partial k}{\partial x_j} = \frac{\partial}{\partial x_j}\left[\left(\mu + \frac{\mu_t}{\sigma_k}\right)\frac{\partial k}{\partial x_j}\right] + \rho P_k - \rho \omega k \tag{4}$$

$$\rho U_j \frac{\partial \omega}{\partial x_j} = \frac{\partial}{\partial x_j}\left[\left(\mu + \frac{\mu_t}{\sigma_\omega}\right)\frac{\partial \omega}{\partial x_j}\right] + C_{\omega 1}\rho P_k \omega - C_{\omega 2}\rho \omega^2 \tag{5}$$

The production of the turbulent kinetic energy, P_k, in Eqs. (4) and (5), is defined as

$$P_k = -\rho \overline{u_i u_j}\frac{\partial U_j}{\partial x_i} \tag{6}$$

The turbulent viscosity ν_t is defined by

$$\mu_t = \alpha^* \frac{\rho k}{\omega} \tag{7}$$

The coefficient α^* damps the turbulent viscosity causing a low-Reynolds numbers correction, which is given by

$$\alpha^* = \alpha^*_\infty \frac{\alpha^*_0 + \mathrm{Re}_t/R_k}{1 + \mathrm{Re}_t/R_k} \tag{8}$$

The quantity Re_t represents the turbulent Reynolds number defined by

$$\mathrm{Re}_t = \frac{\rho k}{\mu \omega}$$
$$R_k = 6; \quad \alpha^*_0 = \frac{\beta_i}{3}; \quad \beta_i = 0.072; \quad \alpha^*_\infty = 1 \tag{9}$$

In the high Reynolds number from of k–ω model: $\alpha^* = \alpha^*_\infty = 1$.

Thus, the turbulent Reynolds stress tensor and the correlation between velocity and temperature fluctuations are deduced using Boussinesq assumption

$$\overline{u_i u_j} = \frac{2}{3}k\delta_{ij} - \nu_t\left(\frac{\partial U_i}{\partial x_j} + \frac{\partial U_j}{\partial x_i}\right) \tag{10}$$

$$-\rho \overline{u_j \theta} = \alpha_t \frac{\partial T}{\partial x_j} \tag{11}$$

Considering the similarity with molecular transport, the turbulent Prandtl number for thermal transport can be determined by the following equation:

$$\sigma_t = \frac{\mu_t}{\sigma_T} \tag{12}$$

The empirical constants values appearing in the above equations are

$$C_\mu = 0.09, \quad C_{\omega 1} = 0.555, \quad C_{\omega 2} = 0.833, \quad \sigma_k = 2.0,$$
$$\sigma_\omega = 2.0, \quad \text{and} \quad \sigma_T = 1.0.$$

Convection and diffusion terms are discretized by means of POWER LAW schemes, while the pressure velocity coupling is achieved through SIMPLEC algorithm.

All the boundary conditions are summarized in Fig. 1. The jet exit velocity V_j is varied for a given Reynolds number. Constant values are imposed for mean velocity and turbulence quantities at inlet

$$U = 0, \quad V = V_j, \quad T = 293\mathrm{K}; \quad k = 0.02V_j^2, \quad \text{and} \quad \omega = \frac{1}{C\mu}\frac{\varepsilon}{k}$$

The moving wall velocity U_0 results from a surface-to-jet velocity ratio R_{sj} defined by: $R_{sj} = U_0/V_j$. The jet exit and the upper plate are maintained at cold temperature T_C while the moving one is heated up to T_H ($T_C = 293$ K and $T_H = 313$ K). At open boundaries the pressure is kept at atmospheric level.

A two dimensional structural non uniform grid was generated and the grid spacing was made thinner close to the wall, where quite high variables gradients prevail (Fig. 1). The convergence of the distribution of the local Nusselt number along the moving wall

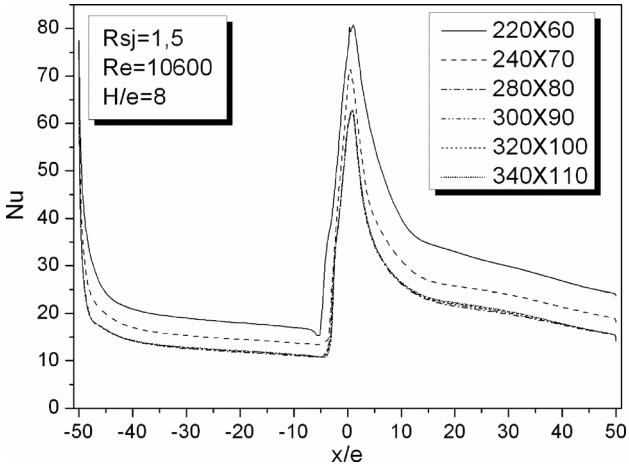

Fig. 2 Effect of grid refinement on the local Nusselt number along the moving wall

with grid refinement is shown in Fig. 2. It observed the grid independence is achieved at 280×80 nodes distribution beyond which no further significant change in Nusselt number distribution is noticed. The grid distribution is consequently used in all following calculations.

3 Numerical predictions and discussion

Several flow structures and heat transfer patterns resulting from the interaction of a confined slot jet with a hot moving wall were numerically studied using a one point closure turbulence model. The parameters considered in this paper of flow interaction are: ratio of plate-jet exit velocity R_{sj} ($0 \le R_{sj} \le 4$) and Reynolds number ($10{,}000 \le \mathrm{Re} \le 25{,}000$). The results show that the topologies of flow and heat transfer are significantly affected by the movement of the impinging wall.

3.1 Validation of Numerical Method. The computed mean velocities components (U/V_j) and (V/V_j), for various horizontal sections (y/e), are concordant with the experimental measurements particle image velocimetry of Senter [15]. With a still wall ($R_{sj} = 0.0$), velocity profiles are symmetric, hence the effect of a moving wall is illustrated by the asymmetry of those profiles (Fig. 3).

3.2 Flow Structure. The computed streamline contours using the k–ω model are plotted in Fig. 4. They correspond to surface-to-jet velocities ratios of $0 \le R_{sj} \le 4$ for $\mathrm{Re} = 10{,}600$ and $H/e = 8$. There is a good agreement between numerical predictions and experimental data of Senter [15] for $0 \le R_{sj} \le 1.0$. Several types of flow structure were observed depending on the surface-to-jet velocity ratio R_{sj}. The first case for $R_{sj} = 0.0$ represents the topology of a confined turbulent jet impinging immobile wall. The streamlines are perfectly symmetric to the jet axis. Two identical eddies appear at both sides of the jet. This pair of vortices was similar to those of both experimentally by Gupta [19] and Senter [15] and through numerical prediction by Beaubert [20] using LES, Abide [21] and Hattori and Nagano [22] through direct numerical simulation, and Senter [15] and Sharif and Banerjee [16] by means of a two equations RANS (k–ε) turbulence model. The second case corresponds to $R_{sj} = 0.25$. The jet is slightly deflected toward the same direction of the plate movement. A third eddy appears on the left part, counter-rotating to the main vortex. For $R_{sj} = 0.5$, the size of the left main recirculation area is significantly influenced, while a new vortex completely emerges. $R_{sj} = 1$, the jet is strongly deflected toward the direction of the plate movement, increasing the size of the new vortex and compressing the left main recirculation area. For high surface-jet velocity ratios of $R_{sj} = 1.5$ and 1.75, the jet is completely carried away by the plate movement, while a new recirculation area gradually emerges compressing one. The main left recirculation area reaches the upper wall pushed up by the thickening of the wall jet. For $R_{sj} = 2$, the size of the left main recirculation area shrinks into a single point, located at the coordinates (x/e, y/e) = (-0.07, 3.52). The thickness of the wall jet is greater in its left side than that the right one. For higher ratios of $R_{sj} = 4$, there is no recirculation zone, the flow is completely deflected by the plate motion. It is found out that the flow behavior is not influenced by Reynolds numbers when $\mathrm{Re} \ge 10{,}000$ (turbulent flow). Besides, for the same Reynolds number and jet–plate velocity ratio, the flow behavior of different impinging distances $4 \le H/e \le 10$ is similar to that of $H/e = 8$. The volume of each vortex increases with of the impinging distance. This result is in concordance with the work of Yokobori et al. [23] for the $R_{sj} = 0$ case.

3.3 Mean Pressure Distributions. The jet deflection is also evidenced by Coanda effect. The pressure coefficient C_p along the moving wall is required for further details about the near-wall pressure effect. For more details, Fig. 5 depicts the static pressure coefficient distribution along the moving wall for several jet-plate velocity ratios. We notice that the pressure coefficients exhibit the same shape for each case. The maximum corresponds to the location of the stagnation point; witch is shifted away from the jet axis when the impinging wall moves. The maximum value of the pressure coefficient decreases when the plate velocity increases. This phenomenon is due to the generation of a new recirculation area. For great R_{sj} values, none pronounced peaks is observed because the fluid is completely detached from the moving wall. At the open boundary (exit), atmospheric pressure is attained ($C_p = 0.0$).

3.4 Vorticity Distributions. The vortical structure of a plane impinging jet is illustrated in Fig. 6. As it can be seen, the primary vortices are close to the impinging wall. The penetration of the new recirculation area is highlighted by the secondary vortex as shows the Fig. 6.

3.5 Skin Friction Evolution. The skin friction coefficient C_f is determined by the following equation:

$$C_f = \tau_w / 1/2\rho V_j^2 \quad \text{where} \quad \tau_w = \mu \left.\frac{\partial U}{\partial y}\right|_{\text{ywall}} \tag{13}$$

The wall friction is certainly useful for the understanding of the near-wall mechanisms. It can be useful in many industrial devices [24]. Figure 7 illustrates the effect of the plate movement ($0 \le R_{sj} \le 4$) for the friction coefficient for Reynolds number of $\mathrm{Re} = 10{,}600$. For all tested cases ($R_{sj} \ge 0$), the skin friction coefficient at the left end ($X/e = -50$) reaches a maximum value which increases with the Rsj ratio. These maxima result from the discontinuity of the velocity between the mobile plate and still part (see Fig. 1). For further details of Fig. 7, we suggest to separately represent the skin friction coefficient around the impinging region ($-20 \le X/e < 20$) for three plate—velocity ratio ranges ($0 \le R_{sj} \le 1$; $1.25 \le R_s \le 1.75$, and $2 \le R_{sj} \le 4$).

For the immobile wall case, the skin friction coefficient is characterized by a minimum at the stagnation point and two symmetrical maxima on both sides of the jet axis [16]. Whereas, for the moving wall cases, we observe (1) a sudden decrease of the local skin friction coefficient at the detachment point of the new recirculation area; (2) the left side maximum increases with the velocity ratio. The effect of Reynolds number on the skin friction coefficient was also investigated. For all jet—plate velocity ratios, the location of the maximum does not seem to be influenced by the Reynolds number, and the increase of the latter brings about a slight decrease of C_f [25,26].

The mean skin friction coefficient is deduced by the following equation:

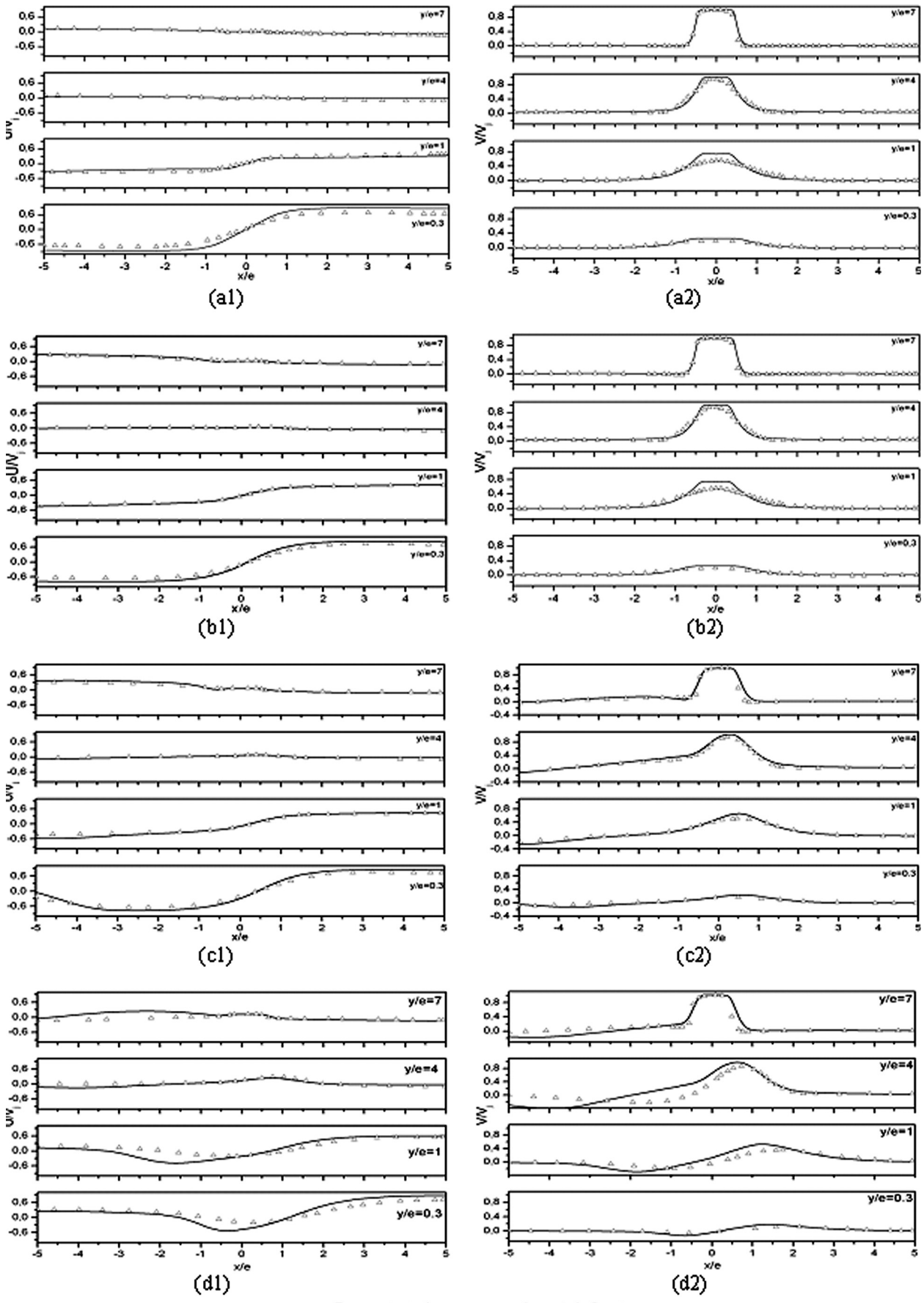

Fig. 3 Mean velocities components U/V_j and V/V_j. ($H/e = 8$, Re = 7850; (*a*), $R_{sj} = 0$, (*b*) $R_{sj} = 0.25$, (*c*) $R_{sj} = 0.5$, and (*d*) $R_{sj} = 1$.

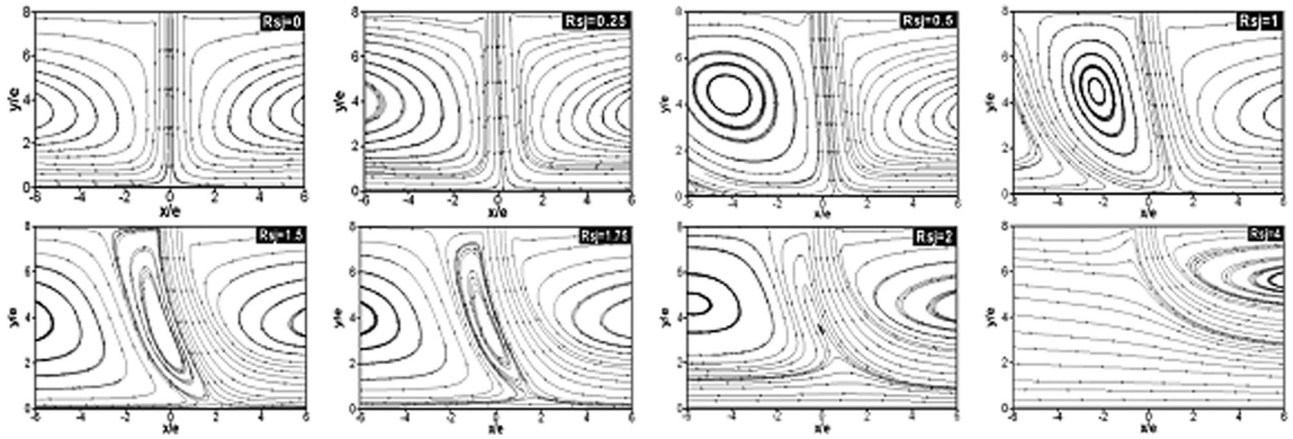

Fig. 4 Streamlines contours: Effect of plate—velocity ratio $H/e = 8$, Re = 10,600 and $0 \leq R_{sj} \leq 4$

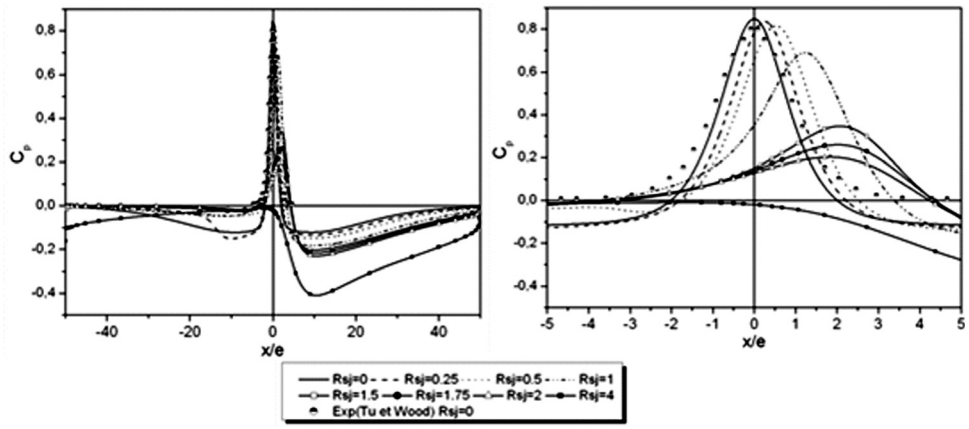

Fig. 5 Pressure coefficient along the moving wall: Effect of plate—velocity ratio $H/e = 8$, Re = 10,600 and $0 \leq R_{sj} \leq 4$

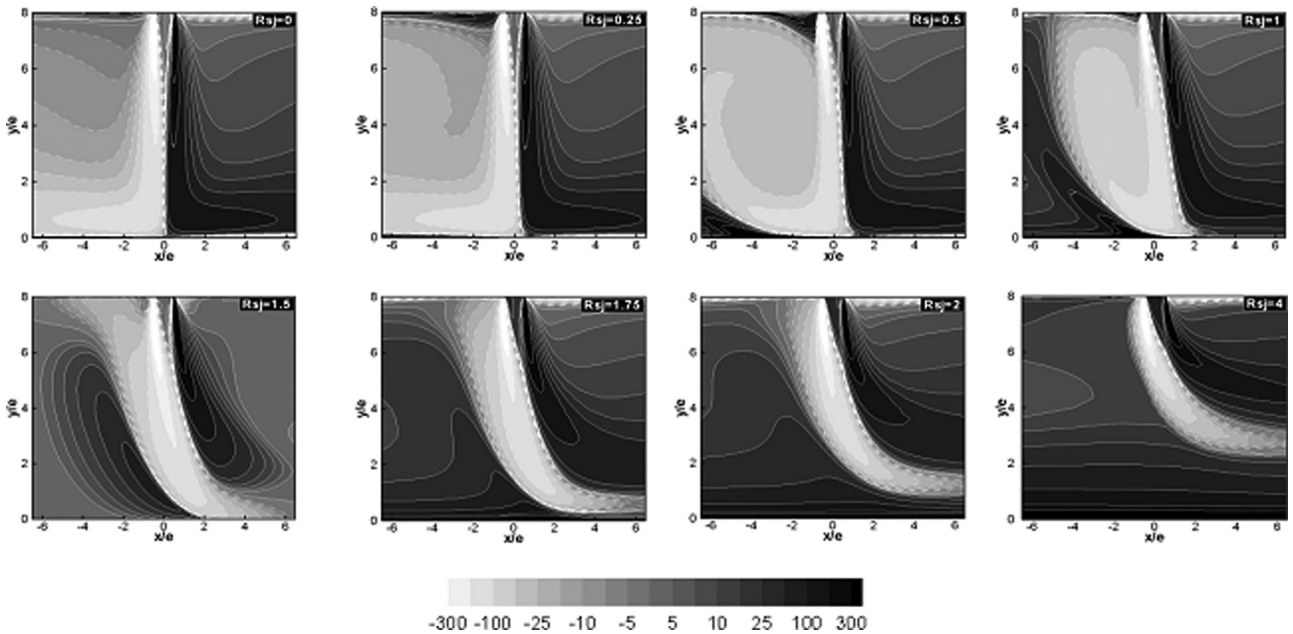

Fig. 6 Vorticity contours: Effect of plate—velocity ratio

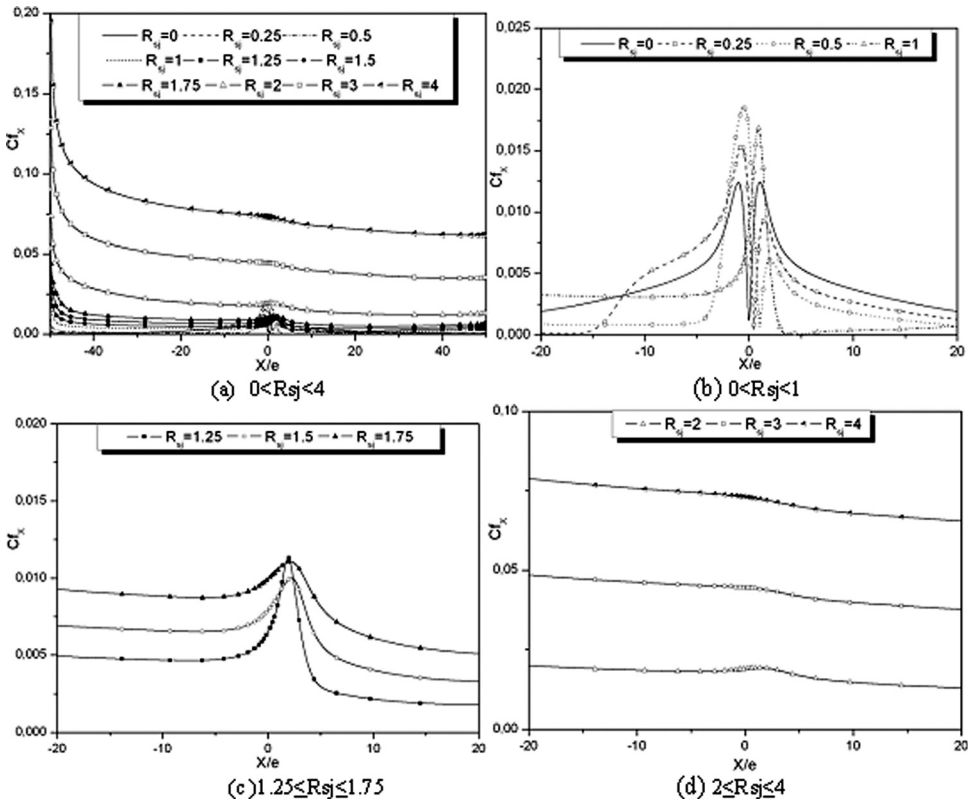

Fig. 7 Skin friction coefficient: Effect of plate—velocity ratio $H/e = 8$, Re = 10,600 and $0 \le R_{sj} \le 4$ (*a*) $0 \le R_{sj} \le 4$; (*b*) $0 \le R_{sj} \le 1$; (*c*) $1.25 \le R_{sj} \le 1.75$; and (*d*) $2 \le R_{sj} \le 4$

$$\overline{C_f} = \frac{1}{L}\int_{-L/2}^{L/2} C_f dx \tag{14}$$

Figure 8 illustrates the average skin friction coefficient variation according to the velocity ratio. This parameter decreases when $R_{sj} = 1$, and increases with the increase of R_{sj} ratios; $(0 \le R_{sj} \le 4)$.

The evolution of the average skin friction coefficient according to the velocity ratio for each Reynolds number within the range of study is correlated by the expressions (14) for two ranges of R_{sj}

$$\begin{aligned} 0.25 \le R_{sj} \le 1 &: \overline{C_f} = 2.102\,x\,10^{-3}\mathrm{Re}^{0.01}R_{sj}^{-0.45} \\ 1 \le R_{sj} \le 4 &: \overline{C_f} = 1.995x10^{-3}\mathrm{Re}^{0.03}R_{sj}^{1.993} \end{aligned} \tag{15}$$

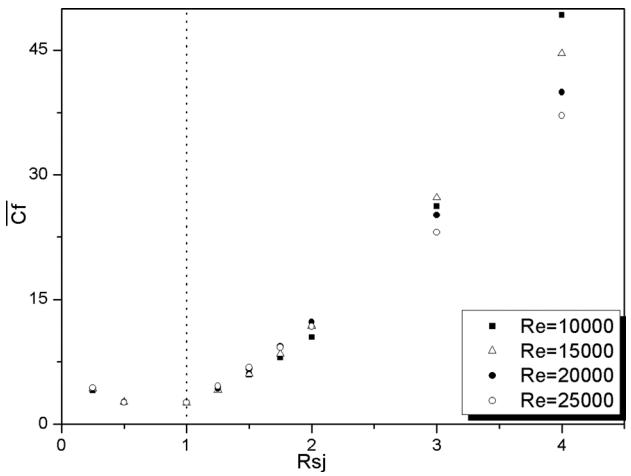

Fig. 8 Mean skin friction coefficient $H/e = 8$

3.6 Local Nusselt Number. The local Nusselt number along the impinging plate Nu(x) is calculated from the following equation:

$$\mathrm{Nu}(x) = -\left(\frac{e}{T_H - T_C}\right)\left(\frac{\partial T}{\partial y}\right)_{ywall} \tag{16}$$

And the average Nusselt along the moving wall is also deduced from the following equation:

$$\overline{\mathrm{Nu}} = \frac{1}{L}\int_{-L/2}^{L/2} \mathrm{Nu}(x)dx \tag{17}$$

Figure 9 exhibits a good agreement with the experimental outcome of Gardon and Akfirat [3] and the numerical results of Senter [15] for a still wall. Figure 9 illustrates the local Nusselt number evolution along the moving wall, for various values of R_{sj}.

Figure 10(*b*) is an enlargement of Fig. 10(*a*) for a more accurate description. The analysis of these curves drives the following conclusions:

— For $R_{sj} = 0$, the curve has a symmetrical bell the shape. The maximum is observed at the stagnation point of the jet. Beyond that, the local Nusselt number symmetrically decreases on both sides of the jet.

— For $0.25 \le R_{sj} \le 1.5$:

- The maximum value decreases and the stagnation point location is shifted toward the same direction as the plate velocity.
- The value decreases in the left part of the plate; this reduction is coupled to the creation of a new recirculation area [15,16].
- A pronounced peak appears at the left end of the moving wall ($X/e = -50$), which augments when R_{sj} increases. The development of this maximum can be explained by the velocity discontinuity between the moving part and the left side still part [15].

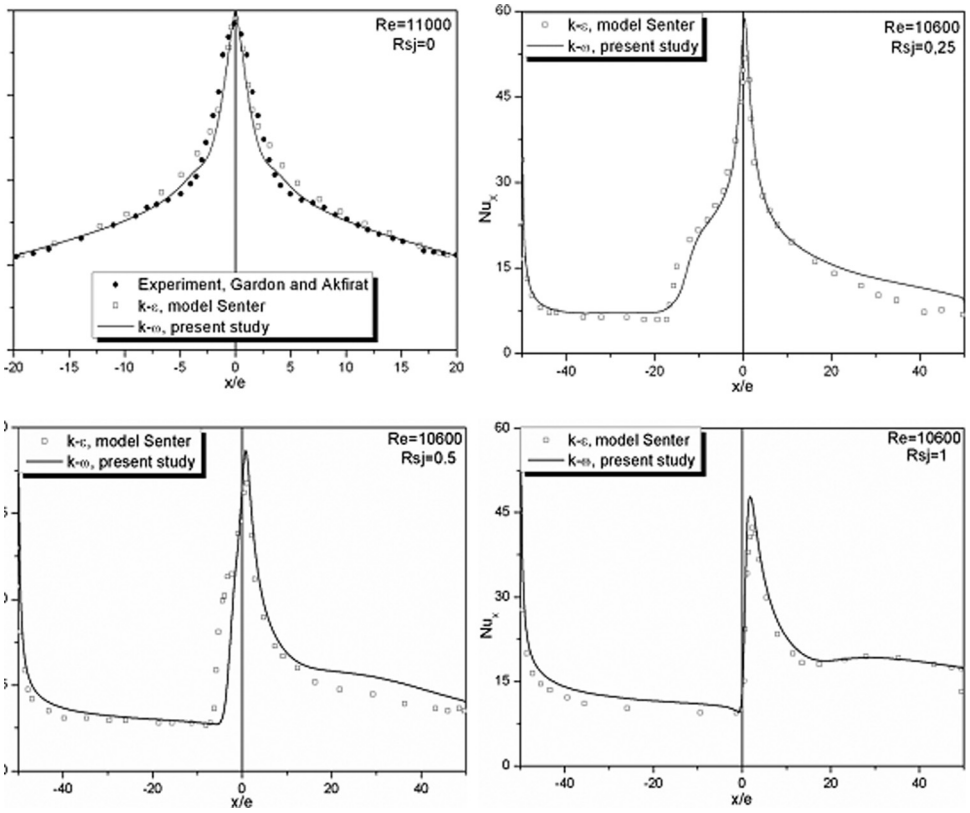

Fig. 9 Validation: Effect of R_{sj} on the local Nusselt number along the hot wall

- The Nusselt number increases on the right side part of the plate when R_{sj} augments due to the effect of a progressive jet deviation.

— For $1.75 \leq R_{sj} \leq 4$: the absence of any obvious peak because the flow completely runs away from the plate. The locations and the maximum values for different R_{sj} are reported in Table 1.

The effect of Reynolds numbers on local Nusselt numbers, for Reynolds numbers, ranging from 10,000 to 25,000, for several R_{sj} $(0 \leq R_{sj} \leq 4)$, was examined. Similar variations are obtained except that their maximum values increase with Reynolds numbers. The stagnation point location does not seem to be influenced by the Reynolds number.

Figure 11 shows the average Nusselt number variation according to the velocity ratios. The average Nusselt number decreases until $R_{sj} = 1.5$; increases for higher values of velocity ratios (R_{sj}). The minimum value of mean skin friction coefficient is reached for $R_{sj} = 1$ case (Fig. 8) but that of average Nusselt number corresponds to $R_{sj} = 1.5$. Fluid flow and thermal fields are not similar which can be explained by the pressure effects (Coanda) which

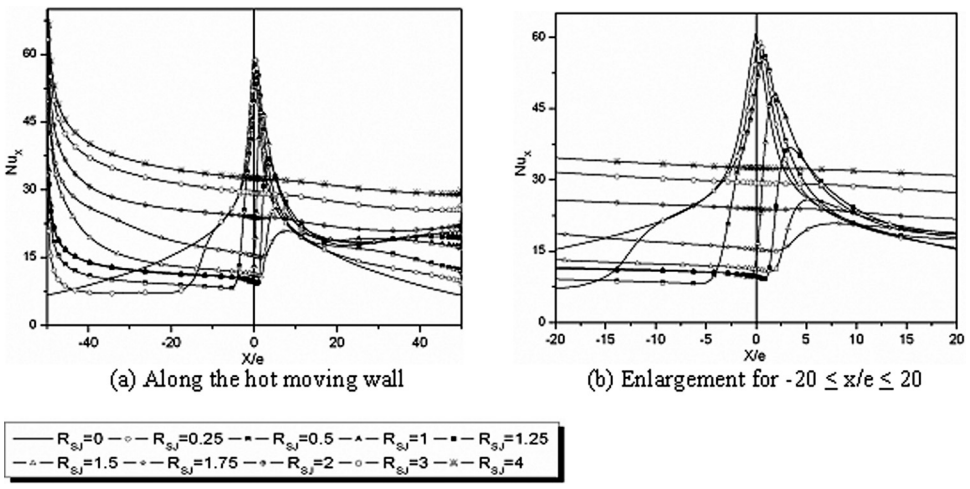

Fig. 10 Distribution of local Nusselt number for $H/e = 8$, Re = 10,600 and $0 \leq R_{sj} \leq 4$ (*a*) Along hot moving wall and (*b*) for $-20 \leq x/e \leq 20$

Table 1 Effect of surface-to-jet velocity on the maximum values of the local Nusselt number and the location of stagnation point. Re = 10,600, *H*/*e* = 8.

R_{sj}	0	0.25	0.5	1	1.25	1.5
X_0/e	0	0.434	0.784	1.837	3.450	5.552
Nu_{max}	61.047	58.796	56.000	47.849	36.796	25.945

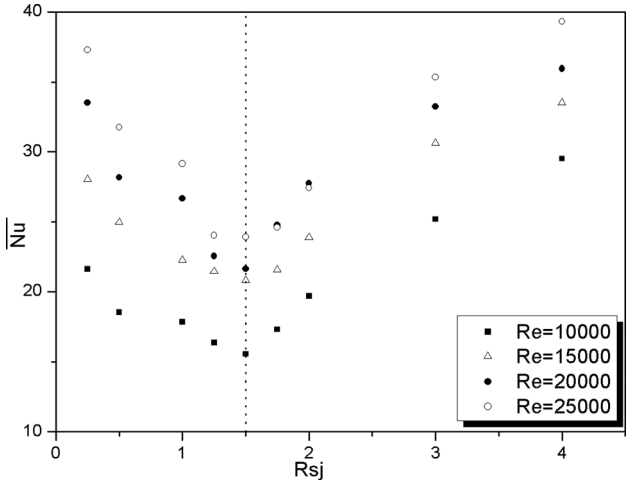

Fig. 11 Average Nusselt number distribution for *H*/*e* = 8

intervene only in the momentum equations, delaying the reattachment process in comparison with thermal behavior.

The average Nusselt number evolution according to the velocity ratios, for each Reynolds number, is correlated by the expressions (17) for two ranges of R_{sj}

$$\begin{aligned} 0 \le R_{sj} \le 1.5 &: \overline{Nu} = (0.188 - 0.046R_{sj})Re^{0.524} \\ 1.5 \le R_{sj} \le 4 &: \overline{Nu} = (0.073 + 0.035R_{sj})Re^{0.524} \end{aligned} \quad (18)$$

4 Conclusions

The effects of Reynolds numbers, plate velocity and impinging distance, on flow fields and heat transfer were discussed in this paper. Results are in good agreement with experimental measurements and previous numerical works. The contours of different variables (streamlines, isobars, kinetic energy, shear stress and vorticity) are symmetrical for unmoving wall cases ($R_{sj} = 0$), and become asymmetric in the case of a moving wall ($R_{sj} \neq 0$). The deviation of the stagnation point from the jet exit axis generates an important variation of the heat transfer. For high velocity ratios ($R_{sj} \geq 2$), there are no stagnation points because the flow is completely detached away from the wall. Many correlations are proposed for several ranges of jet to wall velocity ratios. Additionally, one must emphasize the occurrence of a difference between the corresponding R_{sj} of the minimum value of mean skin friction coefficient ($R_{sj} = 1$) and that of mean Nusselt number ($R_{sj} = 1.5$); which can be explained by the pressure effects (Coanda) which intervene only in the momentum equations, delaying the reattachment process in comparison with thermal behavior.

Nomenclature

C_f = skin friction coefficient
$\overline{C_f}$ = mean skin friction
C_p = pressure coefficient
e = nozzle width (m)
H = impinging distance (m)
k = turbulent kinetic energy ($m^2\ s^{-2}$)
L = length of the impingement plate (m)
Nu_x = local Nusselt number
$\overline{Nu}$ = average Nusselt number
P = mean pressure (Pa)
Pr = Prandlt number
Re = Reynolds number

Greek Symbols

ρ = fluid density ($Kg\ m^{-3}$)
μ = dynamic viscosity of fluid ($Kg\ m^{-1}\ s^{-1}$)
μ_t = turbulent eddy viscosity ($Kg\ m^{-1}\ s^{-1}$)
ω = specific dissipation rate (s^{-1})
Ω = vorticity (s^{-1})
V_j = jet exit velocity exit ($m\ s^{-1}$)
U^+ = nondimensional velocity
U_0 = wall velocity ($m\ s^{-1}$)
U_i = mean velocity components ($m\ s^{-1}$)
u_j = fluctuating velocity components ($m\ s^{-1}$)
V = mean velocity in the y-direction ($m\ s^{-1}$)
x_i = coordinate directions (m)
y^+ = nondimensional distance
R_{sj} = surface-to jet velocity ratio
T = mean temperature (K)
U = mean velocity in the x-direction ($m\ s^{-1}$)

Subscripts

C = cold temperature
H = hot temperature
t = turbulent

References

[1] Abramovich, G. N., 1963, *The Theory of Turbulent Jets*, The MIT Press, Cambridge, MA.
[2] Metzger, D. E., 1962, "Spot Cooling and Heating of Surfaces With High Velocity Impinging Air Jets," Technical Report No. 52, Department of Mechanical Engineering, Stanford University, Stanford, CA.
[3] Gardon, R., and Akfirat, J. C., 1966, "Heat Transfer Characteristics of Impinging Two-Dimensional Air Jets," Trans. ASME J. Heat Transfer, pp. 101–108.
[4] Yap, C. R., 1987, "Turbulent Heat and Momentum Transfer in Recirculating and Impinging Flows," Ph.D. thesis, Faculty of Technology, University of Manchester, Manchester, UK.
[5] Ashforth-Frost, S., Jambunathan, K., and Whitney, C. F., 1997, "Velocity and Turbulence Characteristics of a Semi-Confined Orthogonally Impinging Slot Jet," Exp. Therm. Fluid Sci., **14**, pp. 60–67.
[6] Cziesla, T., Biswas, G., Chattopadhyay, H., and Mita, N. K., 2001, "Large-Eddy Simulation of Flow and Heat Transfer of an Impinging Slot Jet," Int. J. Heat Fluid Flow, **22**, pp. 500–508.
[7] Sahoo, D., and Sharif, M. A. R., 2004, "Numerical Modeling of Slot-Jet Impingement Cooling of a Constant Heat Flux Surface Confined by a Parallel Wall," Int. J. Therm. Sci., **43**, pp. 877–887.
[8] Kadem, N., Mataoui, A., Salem, A., and Younsi, R., 2007, "Numerical Simulation of Heat Transfer in an Axisymmetric Turbulent Jet Impinging on a Flat Plate," Adv. Model. Optim., **9**, pp. 207–217.
[9] Abishek, S., and Narayanaswamy, 2012, "Coupled Effects of Surface-Radiation and Buoyancy on Jet-Impinging Heat Transfer," ASME J. Heat Transfer, **134**, p. 082203.
[10] Subba Raju, K., and Schlünder, E. U., 1977, "Heat Transfer Between an Impinging Jet and a Continuously Moving Surface," Wärme-Stoffübertr, **10**, pp. 131–136.
[11] Huang, P. G., Mujumdar, A. S., and Douglas, W. J. M., 1984, "Numerical Prediction of Fluid Flow and Heat Transfer Under a Turbulent Impinging Slot Jet With Surface Motion and Crossflow," ASME Paper NO. 84-WA/HT-33.
[12] Zumbrunnen, D. A., 1991, "Convective Heat and Mass-Transfer in the Stagnation Region of a Laminar Planar Jet Impinging on a Moving Surface," ASME J. Heat Transfer, **113**, pp. 563–570.
[13] Chattopadhyay, H., Biswas, G., and Mitra, N. K., 2002, "Heat Transfer From a Moving Surface Due to Impinging Slot Jets," ASME J. Heat Transfer, **124**, pp. 433–440.
[14] Chattopadhyay, H., and Saha, S. K., 2003, "Turbulent Heat Transfer From a Slot Jet Impinging on a Moving Plate," Int. J. Heat Fluid Flow, **24**, pp. 685–697.

[15] Senter, J., 2006, "Analyse Expérimentale et Numérique des Écoulements et Des Transferts de Chaleur Convectifs Produits par un jet Plan Impactant une Plaque Plane Mobile," Ph.D. thesis, University of Nantes, Nantes, France.
[16] Sharif, M. A. R., and Banerjee, A., 2009, "Numerical Analysis of Heat Transfer Due to Confined Slot-Jet Impingement on a Moving Plate," Appl. Therm. Eng., **29**, pp. 532–540.
[17] Zumbrunnen, D. A., Incropera. F. P., and Viskanta, R., 1992, "A Laminar Boundary Layer Model of Heat Transfer Due to a Nonuniform Planar Jet Impinging on a Moving Plate," Wärme-und Stoffübertragung, **27**, pp. 311–319.
[18] Wilcox, D. C., 1998, *Turbulence Modeling for CFD*, DCW Industries, Inc., La Canada, CA.
[19] Gupta, S., 2005, "Experimental Analysis of the Dynamical Behaviour and Effectiveness of Air Curtains Designed for Cellular Confining," Ph.D. thesis, University of Nantes, Nantes, France.
[20] Beaubert, F., and Viazzo, S., 2003, "Large Eddy Simulations of Plane Turbulent Impinging Jets at Moderate Reynolds Numbers," Int. J. Heat Fluid Flow, **24**, pp. 512–519.
[21] Abide, S., 2005, "A Domain Decomposition Method Designed for Direct Numerical Simulation: Contribution to Plane Impinging Jets," Ph. D. thesis, University of Nantes, Nantes, France.
[22] Hattori, H., and Nagano, Y., 2004, "Direct Numerical Simulation of Turbulent Heat Transfer in Plane Impinging Jet," Int. J. Heat Fluid Flow, **25**, pp. 749–758.
[23] Yokobori, S., Kasagi, N., and Hirata, M., 1977, "Characteristic Behaviour of Turbulence in the Stagnation Region of a Two-Dimensional Submerged Jet Impinging Normally on a Flat Plate," Proceedings of Symposium on Turbulent Shear Flows, University Park, PA, pp. 3.17–3.25.
[24] Benmouhoub, D., 2011, "Simulation numérique d'un jet plan turbulent impactant une paroi mobile," Thèse de magister, USTHB, Algiers, Algérie.
[25] Tu, C. V., and Wood, D. H., 1996, "Wall Pressure and Shear Stress Measurements Beneath an Impinging Jet," Exp. Thermal Fluid Sci, **13**, pp. 364–373.
[26] Zhe, J., and Modi, V., 2001, "Near Wall Measurements for a Turbulent Impinging Slot Jet," ASME J. Fluids Eng., **123**, pp. 112–120.